Multi-User MIMO Enabled Virtual Reality in IEEE 802.11ay WLAN

Jiayi Zhang, Steve Blandino, Neeraj Varshney, Jian Wang, Camillo Gentile, Nada Golmie
Wireless Networks Division, National Institute of Standards and Technology, Gaithersburg, MD 20899 USA
Emails: {jiayi.zhang, steve.blandino, neeraj.varshney, jian.wang, camillo.gentile, nada.golmie}@nist.gov

2022 IEEE Wireless Communications and Networking Conference (WCNC) | 978-1-6654-4266-4/22/$31.00 ©2022 IEEE | DOI: 10.1109/WCNC51071.2022.9771778

***Abstract*—Virtual reality (VR) coupled with 360° video has been used in a variety of areas, including gaming, remote learning, and healthcare, among others. The 360° video on which VR applications are based today is mostly low resolution and, in order to improve the user experience, bandwidth requirements must increase significantly. Spatial multiplexing (SM) at millimeter wave (mmWave) is an enabling technology introduced in IEEE 802.11ay to support high throughput applications. However, since IEEE 802.11ay commercial off-the-shelf devices are not yet available and the cost for implementation of mmWave testbeds is prohibitive, the expected SM performance in a real application is still unknown. In this paper, we design a mmWave multi-user (MU)-multiple-input multiple-output (MIMO) link-level high fidelity simulation platform, based on IEEE 802.11ay, which is shared as an open source code package. Our simulation platform consists of a measurement-based mmWave channel model and a digital transceiver. To support VR applications, we design the analog-digital hybrid precoders and combiners, enabling SM for MU-MIMO transmissions. We provide an extensive evaluation of the IEEE 802.11ay PHY in terms of throughput and error rates. Our platform reveals that in a living room environment, two users can support up to four streams achieving more than 20 Gbit/sec data-rate per user, enabling the transmission of uncompressed 4K videos.**

I. Introduction

The saturation of the sub-6 GHz bands has forced the exploration of millimeter wave (mmWave) bands as part of the 5G revolution. mmWave technology is at the core of the development of wireless local area networks (WLANs) – building upon the IEEE 802.11ad standard introduced in 2012 – since the IEEE 802.11 Task Group ay (TGay) ratified new physical layer (PHY) and medium access control (MAC) specifications to exploit the spectrum available at 60 GHz. IEEE 802.11ay supports bit rates up to 100 Gbit/sec, using technical advancements such as single-user (SU) and multi-user (MU)-multiple-input multiple-output (MIMO), enabled by the usage of phased array antennas (PAAs) [1], wide bandwidth obtained through channel aggregation and channel bonding, and orthogonal frequency division multiplexing (OFDM) waveform.

Some efforts have been carried out thus far to examine the PHY performance of IEEE 802.11ay systems. For example, Silva *et al.* [2] evaluated the performance of the IEEE 802.11ay single-carrier (SC) mode based on a single data stream between the transmitter and the receiver; Bodi *et al.* [3] studied the performance of the OFDM mode for SU-MIMO. Both demonstrated that due to the intrinsic properties of mmWave propagation, achieving reliable and ubiquitous coverage is a non-trivial task even for short-distance communications, and it requires a detailed system design for each use case. For instance, Chen *et al.* [4] studied the fixed wireless access use case to enable different deployment scenarios, such as broadband residential access, Wi-Fi access point (AP), small cell backhaul, and home media sharing.

One of the use cases proposed by IEEE TGay that has not been yet investigated is the support for virtual reality (VR) head-mounted displays (HMDs). While VR has become an important tool for recreational gaming [5], it is expected to have a positive impact on quality of life as a transferable asset to other areas, including healthcare and education, among others. Together with VR, 360° video can engage users to a unique immersive viewing experience, enhancing the experience of remote location. VR HMD systems are deployed mainly for indoor environments both in private and public spaces, such as in living rooms, but also in public commuter trains [6]. In both environments, the IEEE 802.11ay system performance is bounded by interference from other IEEE 802.11ay devices; for example, other passengers using VR headsets and smartphones. Despite being a semi-stationary scenario, users move their head in response to content; since PAAs synthesize directional beam patterns, a different head orientation may affect the link quality, and in turn the user experience. The indoor VR scenario is particularly interesting to investigate as the spatial multiplexing (SM) feature of the IEEE 802.11ay PHY allows transmission of up to eight independent spatial streams. These streams can be allocated either to a single user or to multiple users. On one hand, the SU-MIMO transmission mode enables a high data-rate for each user, but multiple users need to be allocated on different time slots; on the other hand, using MU-MIMO mode, each user accesses a lower data-rate but multiple users can be served simultaneously. To the best of our knowledge, this trade-off and, more in general, the SM performance of IEEE 802.11ay has not been investigated in the past.

In this paper, we therefore investigate a VR system and the SM schemes adopted by IEEE 802.11ay to support high throughput applications. Our study is enabled by the implementation of an end-to-end mmWave MU-MIMO simulation platform, which is shared as an open source code package in [7]. The simulation platform is composed by a channel model specific to mmWave radio frequency and a novel IEEE 802.11ay PHY digital transceiver model. The main contributions of this paper can be summarized as follows:

1) We design a mmWave MU-MIMO open source package that is conformant to IEEE 802.11ay standard.

2) We analyze the SU/MU-MIMO trade-off by studying the theoretical ergodic spectral efficiency (SE) bounds of different MIMO schemes in a VR indoor applications. Yet, our system design is generic enough to support system-level simulation for other applications as well.
3) We conduct an extensive evaluation of the PHY performance in terms of bit error rate (BER), packet error rate (PER) and data-rate for VR applications.

The remainder of the paper is organized as follows. In Section II, we review quality-of-service requirements for VR applications and multi-stream transmission in IEEE 802.11ay. In Section III, we present the link-level simulation platform. In Section IV, we present the performance of the VR use case in terms of SE, BER, PER and data-rate. Section V concludes the paper.

II. The VR Use Case of IEEE 802.11ay

A. Quality-of-Service Requirements

VR applications have demanding performance requirements in terms of throughput, delay and power consumption, to ensure a high-quality immersive user experience. The 360° video on which VR applications are based today is mostly low resolution but, as display quality is evolving to high definition, the bandwidth requirements will increase significantly. To successfully recreate a real-life experience with streaming 360° VR content, Moving Picture Experts Group (MPEG) recommends a 3D-4K video, i.e., 12K ($11\,520 \times 6\,480$) high-quality spatial resolution [8]. Moreover, VR applications are extremely sensitive to delay to prevent adverse effects, like dizziness or nausea, also known as cyber-sickness, hence a minimum temporal refresh rate of 90 frames per second has been recommended [8]. Moreover, only uncompressed or lightly compressed video can meet the latency requirements [5]. These requirements can be converted to data-rate demands of several Gbit/sec, even after applying state-of-the-art high efficiency video coding (HEVC) compression.

To support wireless VR applications, TGay has introduced video streaming functional and system performance requirements for IEEE 802.11ay devices [9]. TGay devices are required to support lightly compressed 4K and 8K ultra high-definition (UHD) video with data-rate of 1.5 Gbit/sec and 8 Gbit/sec respectively and optionally they may provide a means of supporting uncompressed 4K and 8K UHD video with data-rate up to 18 Gbit/sec and 28 Gbit/sec, respectively. Packet loss rate is set to 10^{-8} to guarantee a fluid experience and the max delay is 10 ms to avoid cyber-sickness.

B. Multi-Stream Transmission

The stringent requirements of data-intensive applications such as VR, have pushed IEEE 802.11ay to introduce new features aimed at improving the system achievable throughput. Among these features, multi-stream transmission increases the spectral efficiency by exploiting the multi-antenna architecture of 60 GHz radios. To this end, hybrid analog-digital architectures are recommended in IEEE 802.11ay, to simplify the hardware complexity by enabling hardware reuse over the antenna

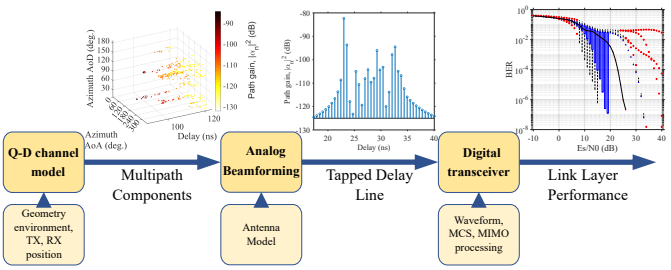

Fig. 1: High-fidelity simulation platform for IEEE 802.11ay

paths. In these architectures, spatial multiplexing is usually achieved with the following steps: (i) The analog beamforming weights, i.e., complex amplitudes applied to the individual antennas of the PAA in order to synthesize an electronic beam in the analog domain, are obtained via the beamforming training procedure [10]. (ii) The receiver estimates the effective channel, i.e., the channel components that fall into the analog beams, using a known pilot sequence. The estimated channel is compressed and feedback to the transmitter [11]. (iii) The transmitter uses the estimated effective channel to design the digital beamforming [11].

III. High-Fidelity Link-Level Model

In this section, we introduce the link-level simulation platform to support VR applications as an example.

A. Architecture

Fig. 1 describes the simulation platform architecture, which consists of three main functional modules: (i) the quasi-deterministic (QD) channel model, (ii) analog beamforming and (iii) digital transceiver. The QD channel model generates the double directional channel impulse response (DDIR), which includes the temporal and angular description of the channel, based on the configured environment layout, the nodes position and the PAA orientations. The analog beamforming module applies the antenna model and the analog beamforming weights at each antenna element to steer the beams, converting the DDIR to the time domain channel impulse response. Subsequently, the channel impulse response is re-sampled at the IEEE 802.11ay sampling rate to obtain the tapped delay line channel. Finally, the digital transceiver uses the channel to conduct link-level simulations.

Our digital transceiver extends the IEEE 802.11ad in the MATLAB WLAN toolbox[1] to be IEEE 802.11ay compliant and it is publicly available at [7]. It supports SU-MIMO and MU-MIMO for both OFDM and SC modes. It also supports several precoder and equalizer options, including singular value decomposition (SVD), zero-forcing (ZF) precoder, block diagonalized-ZF precoder, and minimum mean square error (MMSE) equalizer. The proposed digital transceiver

[1]Certain commercial equipment, instruments, or materials are identified in this paper in order to specify the experimental procedure adequately. Such identification is not intended to imply recommendation or endorsement by the National Institute of Standards and Technology, nor is it intended to imply that the materials or equipment identified are necessarily the best available for the purpose.

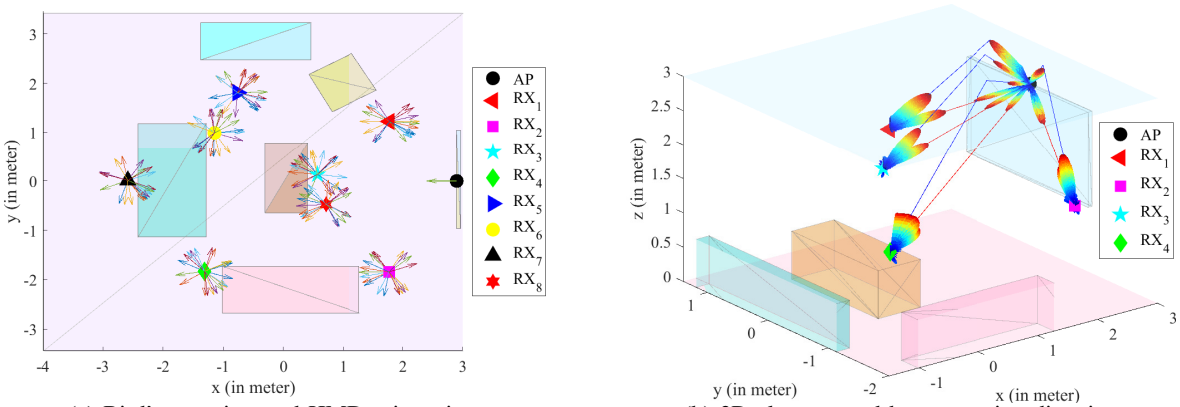

(a) Bird's eye view and HMD orientations

(b) 3D close-up and beam-steering directions

Fig. 2: QD environment for VR applications: a furnished living room of size $7 \times 7\,\mathrm{m}^2$ with a ceiling height of 3 m.

can perform synchronization of the received signal, as well as estimating the channel from the Golay pilot sequences provided in the IEEE 802.11ay packet preamble. In this study, however, we assume perfect knowledge of the channel at both transmitter and receiver to demonstrate the upper bound of the system performance in VR applications. Despite this paper focuses on VR applications, the proposed transceiver implementation supports system-level simulations regardless of the application.

B. QD Channel Model

The QD model consists of deterministic and stochastic multi-path components (MPCs). To describe specular reflections from ambient surfaces, deterministic MPCs are generated through ray tracing given a CAD model of the environment, including the locations of the transmitter and receiver. The stochastic MPCs model diffuse reflections from the rough object surfaces. These are generated from statistical parameters extracted from measurement campaigns [12]. The diffuse reflections tend to cluster in the delay and angle domains around the specular reflections.

In this study, we leverage our open-source ray tracing software [7] to generate the deterministic rays with their diffuse component for a given deployment. In this paper, we consider an indoor living room environment. As shown in Fig. 2, the living room is furnished with multiple couches, tables, and a television set mounted on one of the walls. Each reflector is characterized by unique electromagnetic properties [7]. In this scenario, the AP is located at the top of the television set and facing towards the negative x-direction, while multiple user stations (STAs) have been uniformly generated with an acceptance-rejection method, such that each STA does not coincide with any point of the furniture, as shown in Fig. 2a. We consider a semi-stationary scenario, such that the STA orientation may change. This assumption simulates an user shifting the head in response to a stimulus received from the VR headset. In our modeling, HMD orientations are extracted with a random uniform distribution, such that the azimuth angle $\phi \in [0°, 360°)$ and the elevation angle $\theta \in (-90°, 90°)$, to consider that the neck constraints do not allow the users to move their head in the positive and negative z-directions. Fig. 2a shows each STA and the arrow head represent the projection of the HMDs orientation vectors in the xy plane.

Walls, ceiling, floor and furniture are the scattering sources that generate the multi-path components (MPCs). Using [7], we ray trace all the MPCs up to second-order reflections. Moreover, to form a cluster of rays around each of the reflected rays, the diffuse paths are generated based on measured intra-cluster parameters of the corresponding reflector [13]. The described channel model [7] generates realistic DDIR, which can be formalized as:

$$h_u(t, \tau, \mathbf{\Omega}^{\mathrm{AOD}}, \mathbf{\Omega}^{\mathrm{AOA}}) = \sum_{l=1}^{L_t} a_l(t)\delta(\tau - \tau_l(t),\ \mathbf{\Omega}^{\mathrm{AOD}} - \mathbf{\Omega}_l^{\mathrm{AOD}}(t),\ \mathbf{\Omega}^{\mathrm{AOA}} - \mathbf{\Omega}_l^{\mathrm{AOA}}(t)), \tag{1}$$

where L_t is the number of MPCs at time t, $a_l(t)$ is the complex gain of the l-th path, $\tau_l(t)$ is the path delay, and $\mathbf{\Omega}_l^{\mathrm{AOD}}$ and $\mathbf{\Omega}_l^{\mathrm{AOA}}$ are the 3D angle of departure (AOD) and 3D angle of arrival (AOA) of the l-th path, respectively.

C. Analog Beamforming

In the following, we assume that AP and each STA are equipped with uniform rectangular arrays with M_{AE} and N_{AE} antenna elements, respectively. To perform the hybrid beamforming, we first select the analog beam steering vectors at the AP and at each STA. For this purpose, we assume perfect knowledge of the channel large scale parameters, i.e., power and AOA/AOD of each MPC and we consider ideal phase shifters, which guarantee infinite resolution of the steering angles. Note that full space search is not practical in terms of complexity and time required to achieve an optimal solution. Thus, to find the optimal beam steering directions, we reduce the search space such that the angular codebooks $\mathcal{N}_{\mathrm{STA}}^{u}$ and $\mathcal{N}_{\mathrm{AP}}$, which refer to the codebook at the u-th STA and at the AP respectively, include only the AOA and AOD of line-of-sight (LoS) and first order reflected rays for each AP and u-th STA link.

Since the VR requirements described in Section II aim at guaranteeing a fluid experience at each STA, we design the analog beamforming with the objective to achieve the

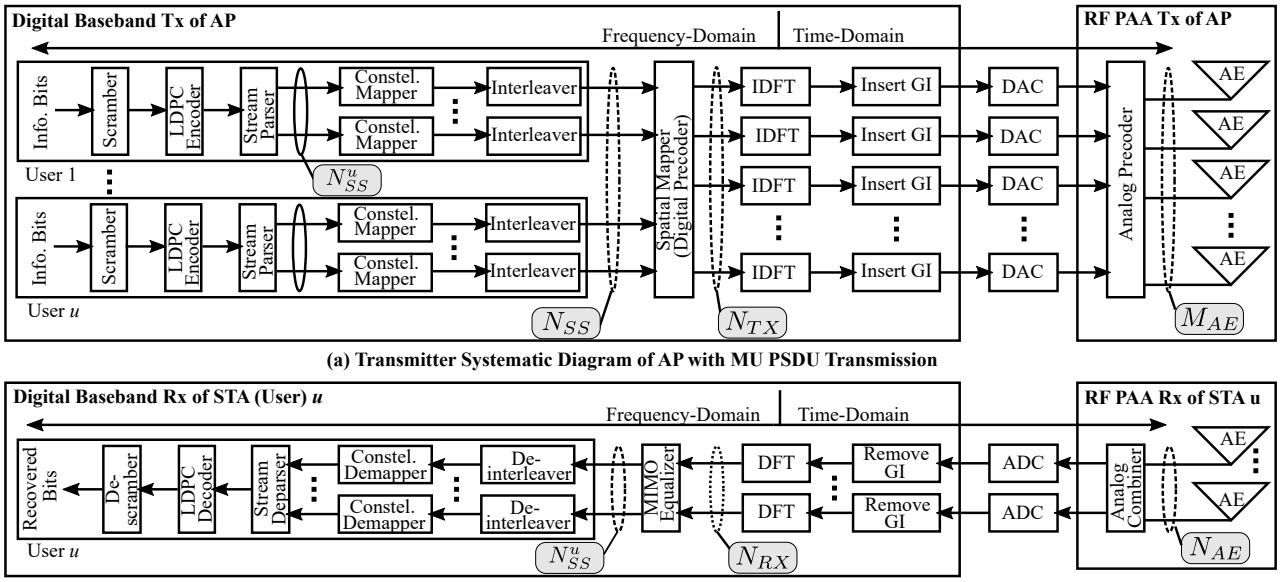

(a) Transmitter Systematic Diagram of AP with MU PSDU Transmission

(b) Receiver Systematic Diagram of STA with MU PSDU Transmission

Fig. 3: Transceiver diagram of IEEE 802.11ay OFDM PHY mode, in MU-MIMO downlink transmission.

minimum requirements at each STA in the system. Hence, we design a max-min algorithm, to maximize the minimum capacity achievable at each STAs. Formally, we compute the instantaneous capacity C_u at each STA u, using the equivalent narrowband channel gain as:

$$C_u = B\log_2\left|\mathbf{I}+\frac{P_{\mathrm{T}}}{\sigma^2}\mathbf{H}_{\mathrm{E}}^{u}\mathbf{H}_{\mathrm{E}}^{u\,H}\right| = B\sum_{j=1}^{N_{\mathrm{SS}}^{u}}\log_2\left(1+\frac{P_{\mathrm{T}}|\lambda_j|^2}{\sigma^2}\right), \quad (2)$$

where B is the channel bandwidth, P_{T} is the transmit power and σ^2 is the thermal noise power of the receiver. The values λ_j denote the singular values of the downlink equivalent channel matrix $\mathbf{H}_{\mathrm{E}}^{u} = \mathbf{W}^{u\,H}\mathbf{H}^{u}\mathbf{F}$, where $\mathbf{H}^{u} \in \mathbb{C}^{N_{\mathrm{AE}}\times M_{\mathrm{AE}}}$ represents the full digital downlink MIMO channel between the AP and the STA u at the time t obtained as $\mathbf{H}^{u} = \mathbf{A}_{\mathrm{AOA}}\mathrm{diag}(h_u)\mathbf{A}_{\mathrm{AOD}}^{H}$, where $\mathbf{A}_{\mathrm{AOA}} \in \mathbb{C}^{N_{\mathrm{AE}}\times L_t}$ and $\mathbf{A}_{\mathrm{AOD}} \in \mathbb{C}^{M_{\mathrm{AE}}\times L_t}$ contain the STAs and AP array response vectors at the angles $\mathbf{\Omega}_{\mathrm{AOA}}$ and $\mathbf{\Omega}_{\mathrm{AOD}}$; $\mathbf{F} \in \mathbb{C}^{M_{\mathrm{AE}}\times N_{\mathrm{Tx}}}$ is the analog beamforming and $\mathbf{W}^{u\,H}$ is the conjugate transpose of $\mathbf{W}^{u} \in \mathbb{C}^{N_{\mathrm{AE}}\times N_{\mathrm{Rx}}}$, which is the analog combiner at the STA u. The optimal analog beamforming $\bar{\mathbf{F}}$ and the optimal analog combiner $\bar{\mathbf{W}}^{u}$ are designed such that:

$$\left\{\bar{\mathbf{F}},\bar{\mathbf{W}}^{u}\right\} = \arg\max_{\mathbf{F},\mathbf{W}}\left\{\arg\min_{u}\quad\{C_u\}\right\}, \quad (3)$$

$$\text{subject to: } \mathbf{F}\in\mathcal{N}_{\mathrm{AP}},\quad [\mathbf{F}]_{i,l}[\mathbf{F}]_{i,l}^{*} = 1/M_{\mathrm{AE}};$$
$$\mathbf{W}^{u}\in\mathcal{N}_{\mathrm{STA}}^{u},\quad [\mathbf{W}^{u}]_{i,l}[\mathbf{W}^{u}]_{i,l}^{*} = 1/N_{\mathrm{AE}};$$

where $[\cdot]_{i,l}$ denotes the i-th row and l-th column of a matrix and $[\cdot]_{i,l}^{*}$ is its complex conjugate i.e., all elements of $\mathbf{F}$ and $\mathbf{W}$ have equal gain. The optimization problem is solved by performing a complete search on the codebooks at AP and each u-th STA. Fig. 2b shows an example of beams designed by solving the optimization problem in Eq. (3). In this example, 4 STAs, each receiving 2 streams from the AP, communicate by exploiting the LoS and the ceiling reflected ray.

D. IEEE 802.11ay Compliant Digital Transceiver

We consider the enhanced directional multi-gigabit (EDMG) OFDM transmission in physical-layer service data unit format [14], i.e., the data-field of the EDMG physical-layer protocol data unit. Fig. 3 shows the baseband MU-MIMO signal processing of the EDMG digital transceiver.

As shown in Fig. 3(a), the modules at the AP transmitter, including scrambler, low-density parity-check code (LDPC) encoder, stream parser and constellation mapper, are operated on a per user basis; while the remaining processing in the transmit chains, including the spatial mapper, inverse digital Fourier transform (IDFT), and cyclic prefix (CP) insertion, are carried out over multiple user's signals jointly [14, Section 28.6.3.1]. The spatial mapping considered in this work is a frequency-domain regularized zero-forcing (RZF) [15] precoding. The digitally precoded MU symbols of each transmit chain are OFDM modulated with a 512 point IDFT, followed by the CP insertion. Finally, the N_{Tx} symbol sequences of all transmit chains are respectively converted by the digital-to-analog converters, weighted by the analog precoding network and sent to the antennas.

The STA receiver procedure is illustrated in Fig. 3(b). After the analog combining and analog-to-digital conversion, the OFDM symbols are demodulated by discrete Fourier transform (DFT) operation followed by the CP removal and a MMSE MIMO equalizer. Subsequently, the constellation demapping, stream deparsing and LDPC decoding are carried out to complete the PHY signal processing procedure. The LDPC encoder and decoder as well as constellation mapper and demapper support a variety of modulation and coding schemes (MCSs) for OFDM mode transmission with different coding rates to comply with the IEEE 802.11ay standard, including dual-carrier modulation (DCM)-binary phase shift keying (BPSK), DCM-quadrature phase-shift keying (QPSK), 16-quadrature amplitude modulation (QAM), and 64-QAM [14].

The digital transceiver implementation is shared as an open source package [7] to support and accelerate the design of future wireless systems.

IV. MU-MIMO Performance Evaluation

In this section, we present simulation results in terms of BER, PER and data-rate.

A. Methodology

We first investigate the theoretical link-level SE bounds of different MIMO schemes considering various SM configurations and PAA sizes, and select the ones that best meet the throughput requirements of VR applications. From the system design point of view, a SE-based analysis provides the general design guideline for link-level configurations, while PHY simulation demonstrates the actual performance. The advantages of using SE instead of the data-rate per MCS directly, owning to the SE analysis can be adopted for simplifying the procedure of system design. By contrast, the calculation of data-rate requires bit-by-bit simulations.

The instantaneous SE of STA u can be computed by summing the SE over its N_{Rx} spatial streams and K_{SD} data subcarriers as a function of the post-equalizer signal-to-interference-plus-noise ratio (SINR). The u-th STA's ergodic SE η_u is the average of its instantaneous SE, which can be expressed as:

$$\eta_u = \mathbb{E}_{\Gamma}\left\{\frac{K}{K+N_{\mathrm{GI}}}\frac{1}{K_{\mathrm{SD}}}\sum_{k=1}^{K_{\mathrm{SD}}}\sum_{j=1}^{N_{\mathrm{Rx}}}\log_2\left(1+\Gamma^{u}_{j,k}\right)\right\}, \qquad (4)$$

where $\Gamma^{u}_{j,k}$ denotes the post-equalizer SINR at subcarrrier k and the spatial stream j of the u-th STA. In addition, the PHY system operates in OFDM mode using a long CP with a length of N_{GI}=192 samples based on K=512-point DFT/IDFT [14].

We assume a MU downlink VR transmission, where the AP is equipped with a PAA of $M_{\mathrm{AE}} = 256$ antenna elements disposed in a 16×16 configuration to guarantee a narrow beam, both in azimuth and elevation planes. Each element has an omni-directional radiation pattern; hence, the array can cover 360° in azimuth plane and 180° in elevation plane. The PAA at AP is fully connected to $N_{\mathrm{Tx}} = 8$ transmitter chains to transmit a maximum of $N_{\mathrm{SS}} = 8$ spatial streams simultaneously. The STAs are equipped with $N_{\mathrm{AE}} = 4$ antenna elements.

We study different SM configurations upon varying the number of STAs U and the number of receiver chains per STA N_{Rx}. We assume that the AP allocates equal power to $N_{\mathrm{SS}} = 8$ spatial streams, and each STA has the same number of receiver chains. We study the performance by varying the number of STAs in the system, such that $U \in \{2, 4, 8\}$. Hence, depending on the number of STA simulated, each STA can be equipped with $N_{\mathrm{Rx}} \in \{1, 2, 4\}$ receiver chains. We refer to the SM configurations to be evaluated as 'U-STA' case for the given combination of U and N_{Rx}. For example, 4-STA case refers to 4 STAs, each with 2 streams.

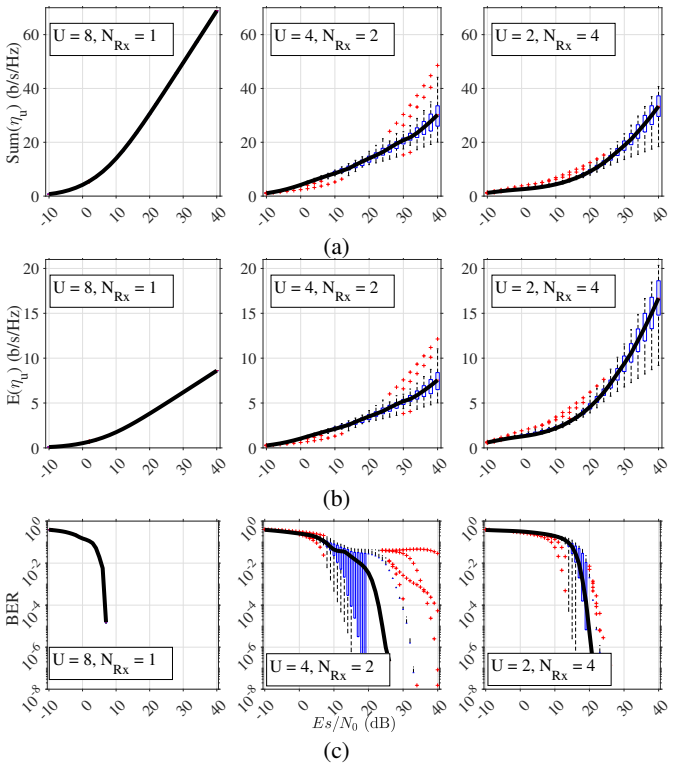

Fig. 4: Varying U, N_{Rx}: (a) Sum Ergodic SE vs SNR (b) Mean Ergodic SE vs SNR (c) BER vs SNR, MCS 6.

B. Evaluation Results

For each simulation SM configuration we simulate 20 different HMD orientations. We provide the statistics of the SE and BER (minimum, maximum, median, 25th and 75th percentile) by using a box-plot at each SNR point. The bottom and top edges of the box indicate the 25th and 75th percentiles, respectively. The whiskers extend to the most extreme data points not considered outliers, and the outliers are plotted individually using the '+' symbol. The center of the box is the median and it shown as a continue black line, to indicate the trend of the results.

1) Impact of the SM and head orientations on SE: We analyze the sum-STA and the mean per-STA ergodic SE over 20 head orientations upon varying the SM schemes.

As shown in Fig 4(a), the 8-STA case achieves the highest sum-STA SE since the AP can allocate the strongest MPC (i.e., the LOS) for each STA. When increasing the spatial multiplexing order per station, the sum SE decreases since the AP exploits, besides the LOS, the reflections of the environment having a larger path loss. While the sum SE achieved in the 4-STA and 2-STA cases is similar, the best sum-STA SE offered by the individual orientation for 4-STA achieves higher rate than the best results of individual orientation for 2-STA. Indeed, when increasing the spatial multiplexing order, weaker reflections are used. Moreover, using a single stream per STA, guarantees a constant SE over the different orientations, since the different LOSs are naturally separated by the geometrical distance among the users. Instead, when transmitting over different MPCs, the head rotation plays a

bigger role, since different radiation patterns, lead to different inter-streams interference.

When designing the MU-MIMO system, a key design choice is the metric to optimize, which mainly depends on the application. A VR system requires fairness among different users, hence a per-STA SE should be preferred. Analyzing the per-STA SE in Fig 4(b), the 8-STA case yields the lowest SE per-STA, since each STA is served with a single stream. By contrast, the 2-STA case represents the SM scheme that guarantees the highest SE per STA. All U-STA cases yield similar performance in the low SNR regime, since the performance are limited by noise rather than interference. However, at the high SNR regime, which is the most natural operating region for an indoor VR system, the 2-STA case is the best choice for optimizing the user experience.

2) Impact of the SM configuration and head orientations on BER: Besides SE, we also study the impact of the SM configuration and head orientations on the BER performance. Fig. 4(c) depicts the behavior of the BER for different head orientations with various SM configurations. We transmit MCS 6, i.e., the symbols are QPSK modulated with a coding rate of one-half. Fixing the number of streams transmitted by the AP such that $N_{\mathrm{SS}} = 8$ spatial streams, we notice that the inter-stream interference is the main factor that impacts BER, as the 8-STA case outperforms the other SM schemes. Thanks to the spatial sparsity of mmWave channels, the inter-user interference among STAs located in different positions can be easily suppressed with a hybrid precoding scheme.

The trend of the 25th percentile of the box-plot, i.e., the bottom of each box, demonstrates that the BER achieved by the individual orientation of the 4-STA cases in general outperforms the one of the 2-STA cases, since the low spatial correlation between inter-user streams. However, because of the three degrees of freedom of the head movement in the VR use case, the interference to be mitigated varies depending on the HDM orientation. Few outlier orientations in 4-STA cases are suffering from high spatial correlation. When high spatial correlation occurs for some orientations, the hybrid precoder may not be able to suppress the interference completely, leading to a BER saturation.

3) Impact of MCS on PER and data-rate: Finally we study the maximum achievable data-rate at different MCSs. Hence, we propose the performance analysis for the orientation configuration achieving the highest data rate. Fig. 5 illustrates the average and individual STA PER and their corresponding achievable data-rate, for a MU-MIMO system with $U = 2$ and $N_{Rx} = 4$.The MCS 1 is capable of achieving 3.46 Gbit/sec average STA data-rate to support lightly compressed 4K UHD video at $E_s/N_0 = 10$ dB. The MCS 16, instead, can achieve the average STA data-rate requirement of 20.72 Gbit/sec to support uncompressed 4K UHD video at SNR higher than 30 dB.

V. Conclusion

Since IEEE 802.11 ay commercial off-the-shelf devices are not yet available, and the cost for implementation of mmWave testbeds is prohibitive, in this paper we have proposed a high-fidelity link-level simulation platform, which includes a realistic channel model, and the full digital transceiver chain including the MU-MIMO signal processing. The proposed link-level simulation platform enables the analysis of the MU-MIMO trade-off between throughput and reliability. As an example, we have proposed the analysis of a VR application. The SE analysis reveals that allocating multiple streams per user is necessary to achieve the VR requirements. The extensive BER/PER evaluation of the IEEE 802.11ay PHY shows that inter-stream interference is the main limiting factor in a mmWave MU-MIMO system. Moreover, the head orientation in a VR application affects the link quality. In the scenario considered, IEEE 802.11ay achieves the average-STA data-rate requirement of more than 20 Gbit/sec at each user, hence, it is able to support uncompressed 4K UHD video. The digital transceiver implementation is shared as an open source package to support and accelerate the design of future wireless systems for both communication and sensing applications.

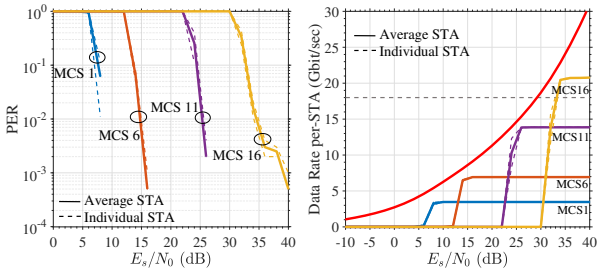

Fig. 5: Gigabit data-rate per STA of 2-STA case vs SNR, upon varying MCS.

References

[1] A. Banerjee *et al.*, "Millimeter-wave transceivers for wireless communication, radar, and sensing," in *Proc. IEEE CICC 2019*, 2019, pp. 1–11.

[2] C. R. C. M. Da Silva *et al.*, "Analysis and simulation of the IEEE 802.11ay single-carrier PHY," in *Proc. IEEE ICC 2018*, 2018, pp. 1–6.

[3] A. Bodi and *et al.*, "Physical-layer analysis of IEEE 802.11ay based on a fading channel model from mobile measurements," in *Proc. IEEE ICC 2019*, 2019, pp. 1–7.

[4] C. Chen *et al.*, "Millimeter-wave fixed wireless access using IEEE 802.11ay," *IEEE Commun. Mag.*, vol. 57, no. 12, pp. 98–104, 2019.

[5] J. Chakareski and *et al.*, "6DOF virtual reality dataset and performance evaluation of millimeter wave vs. free-space-optical indoor communications systems for lifelike mobile VR streaming," in *Proc. ACSSC 2020*.

[6] *IEEE 802.11 TGay Use Cases*, IEEE Std. IEEE 802.11-2015/0625r4.

[7] H. Assasa *et al.* A Collection of Open-source Tools to Simulate IEEE 802.11ad/ay WLAN Networks in Network Simulator ns-3. [Online]. Available: https://github.com/wigig-tools

[8] T. S. Champel *et al.*, "Quality requirements for VR," in *Proc. 116th MPEG Meeting of ISO/IEC JTC1/SC29/WG11*, 2016.

[9] *TGay Functional Requirements*, IEEE Std. IEEE 802.11-2015/1074r0.

[10] C. R. C. M. Da Silva *et al.*, "Beamforming training for IEEE 802.11ay millimeter wave systems," in *ITA 2018 Workshop*, 2018, pp. 1–9.

[11] S. Blandino *et al.*, "Multi-user hybrid MIMO at 60 GHz using 16-antenna transmitters," *IEEE Trans. Circuits Syst. I*, vol. 66, no. 2, pp. 848–858, 2019.

[12] C. Gentile and *et al.*, "Quasi-deterministic channel model parameters for a data center at 60 GHz," *IEEE Antennas Wireless Propag. Lett.*, vol. 17, no. 5, pp. 808–812, 2018.

[13] *IEEE P802.11 Wireless LANs: Channel Models for IEEE 802.11ay*, IEEE Std. IEEE 802.11-15/1150r9, 2015.

[14] *Part 11: Wireless LAN (MAC) and (PHY) Specifications–Amendment 2: Enhanced Throughput for Operation in License-Exempt Bands Above 45 GHz*, IEEE Std. IEEE P802.11ay/D7.0, 2020.

[15] R. W. Heath Jr. and *et al.*, *Foundations of MIMO Communication*. Cambridge University Press, 2018.